Wave-vector filtering effect of the electric–magnetic barrier in HgTe quantum wells*

Zou Yong-Lian(邹永连)[a] and Song Jun-Tao(宋俊涛)[b]†

[a] Institute of Physics, Chinese Academy of Sciences, Beijing 100190, China
[b] Department of Physics and Hebei Advanced Thin Film Laboratory, Hebei Normal University, Shijiazhuang 050024, China

(Received 18 October 2012; revised manuscript received 12 December 2012)

Because of the helicity of electrons in HgTe quantum wells (QWs) with inverted band structures, the electrons cannot be confined by electric barriers since electrons can tunnel the barriers perfectly without backscattering in the HgTe QWs. This behavior is similar to Dirac electrons in graphene. In this paper, we propose a scheme to confine carriers in HgTe QWs using an electric–magnetic barrier. We calculate the transmission of carriers in 2-dimensional HgTe QWs and find that the wave-vector filtering effect of local magnetic fields can confine the carriers. The confining effect will have a potential application in nanodevices based on HgTe QWs.

Keywords: magnetic barrier, topological insulator, helical states, HgTe quantum well

PACS: 73.63.Hs, 73.20.At, 73.23.Ad, 73.40.Gk **DOI:** 10.1088/1674-1056/22/3/037304

1. Introduction

In recent years, HgTe quantum wells (QWs) have aroused a great deal of interest in condensed matter physics due to their potential application in nanodevices.[1–4] The effective Hamiltonian of HgTe QWs has a mass parameter which depends on their thickness.[2] When the thickness is greater than a critical value around 6.3 nm, the mass parameter becomes negative and a quantum phase transition occurs. This phase is a topological phase which possesses a non-trivial topological number and displays the quantum spin Hall effect.[5,6] The quantum spin Hall effect is robust to disorder and has weak electron–electron interaction, as in the quantum Hall effect. In the quantum spin Hall effect, there is a pair of edge states with opposite spins propagating in opposite directions at one edge.[5]

Graphene has also aroused a lot of attention due to its linear dispersion around Dirac points.[7–9] Dirac-like electrons in graphene can tunnel a potential barrier perfectly at normal incidence, which is known as Klein tunneling.[7,8] This unusual behavior is a manifestation of the chirality of Dirac electrons.[8] The perfect tunneling in graphene has two sides. On one side, due to the chirality of Dirac electrons in graphene, the electrons are less affected by disorders and possess high-mobility, however on the other side, it is hard to confine electrons in a potential barrier, which is often used in producing quantum point contacts, quantum dots,[10–12] and so on. Thus, it causes difficulties in producing quantum point contacts[11] in graphene, which affects its application.

Many works have studied how to confine electrons in graphene. To confine Dirac electrons, a magnetic barrier is often used.[11,12] Magnetic barriers have a great wave-vector filtering effect on the Dirac electrons in graphene. There are many kinds of magnetic field configurations in graphene which show a strong filtering effect. Among these configurations, the delta function approximation of magnetic fields is very convenient for calculation and possesses the main physics in confining Dirac electrons.[13]

Carriers in HgTe QWs display a similar behavior[14,15] to the Dirac electrons in graphene. The electrons in HgTe QWs can tunnel barriers perfectly for intra-band tunneling at normal incidence.[14] This behavior may limit its use in nanodevices. For example, the quantum point contact (QPC) which is often generated and manipulated by gate voltages[16] can produce narrow channel width for conventional 2-dimensional electron gas (2DEG) with parabolic dispersion. However, in HgTe QWs, this effective channel width may be broadened because of the tunneling process near the edges of the potential wall. In this paper, we propose a scheme using electric-magnetic barriers to confine electrons in HgTe QWs and calculate the transmission of carriers in two dimensional HgTe QWs. This wave-vector filtering effect makes manipulation of carriers in HgTe QWs more convenient and effective and have potential applications in nanodevices based on HgTe QWs. The rest of our paper is organized as follows. In Section 2, we propose our model and give details of calculation. In Section 3, we discuss our results. At the end, we give a brief summary.

2. Model

As shown in Fig. 1, the system under consideration is a HgTe QW and the electrons are confined in the x–y plane. In the middle region, there is a ferromagnetic strip which will in-

*Project supported by the National Natural Science Foundation of China (Grant Nos. 10821403 and 11047131), the National Basic Research Program of China (Grant No. 2009CB929100), and the Research Fund for the Doctoral Program of Higher Education of China (Grant No. 20101303120005).

†Corresponding author. E-mail: juntao_song@foxmail.com

© 2013 Chinese Physical Society and IOP Publishing Ltd

duce a local magnetic field perpendicular to the 2DEG in HgTe QWs.[12] We assume that the magnetic field at the fringe of the strip is homogeneous along the y direction, and its magnitude can be tuned by an external magnetic field. Since the typical Fermi wavelength of the 2DEG under consideration is much larger than the range of the magnetic field, we can approximate the magnetic field as δ functions,[17,18] i.e.,

$$B_z(x) = Bl_{B_0}(\delta(x) - \delta(x-L)),$$

where l_{B_0} is the typical magnetic length for a typical magnetic strength.[13] When $B_0 = 0.1$ T, $l_{B_0} \simeq 80$ nm. This magnetic field is related to a vector potential in Landau gauge $\boldsymbol{A}(x) = [0, A_y(x), 0]$, where $A_y(x) = Bl_{B_0}(\Theta(x) - \Theta(x-L))$, and $\Theta(x)$ is the Heaviside step function. A voltage barrier can also be induced in the 2DEG if a gate voltage is imposed on the ferromagnetic strip. We assume that the gate voltage $V_g(x) = V_g[\Theta(x) - \Theta(x-L)]$ has a rectangular shape in the middle region.

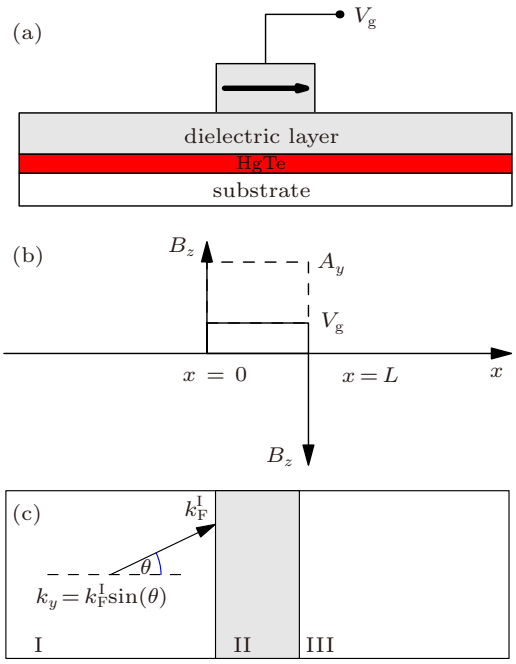


Fig. 1. (color online) (a) Schematic illustration of the HgTe QWs with a ferromagnetic strip. (b) The strip induces a local magnetic field B_z and a voltage barrier V_g. The magnetic fields are localized at $x = 0$ and $x = b$ and A_y is the vector potential of the magnetic fields. (c) The incident electrons are injected from the left leads (region I) with angle θ to the right region (region III) through the barrier (region II). The Fermi wave vector of incident electrons is k_F^I of which the y-component is k_y.

We start from the effective Hamiltonian,[2]

$$H = \epsilon_k \begin{pmatrix} 1 & 0 & 0 & 0 \\ 0 & 1 & 0 & 0 \\ 0 & 0 & 1 & 0 \\ 0 & 0 & 0 & 1 \end{pmatrix} + \begin{pmatrix} M(\boldsymbol{k}) & Ak_- & \mathrm{i}\alpha k_- & 0 \\ Ak_+ & -M(\boldsymbol{k}) & 0 & 0 \\ -\mathrm{i}\alpha k_+ & 0 & +M(\boldsymbol{k}) & -Ak_+ \\ 0 & 0 & -Ak_- & -M(\boldsymbol{k}) \end{pmatrix}, \quad (1)$$

where $\boldsymbol{k} = [k_x, \pi_y]$, $\epsilon_k = C - D(k_x^2 + \pi_y^2)$, $M(\boldsymbol{k}) = M - B(k_x^2 + \pi_y^2)$, $k_\pm = k_x \pm \mathrm{i}\pi_y$ with $\pi_y = k_y + eA_y/\hbar$ in the presence of A_y, A, B, C, and D are structural parameters, M is a mass parameter related to the thickness of HgTe QWs, and α is the Rashba spin–orbit interaction (RSOI) strength. The RSOI can be induced by an external electric field, which causes structural asymmetry. In our calculation,[2] we take $A = 364.5$ meV·nm, $B = -686$ meV·nm^2, $C = 0$, $D = -512$ meV·nm^2, and $M = -10$ meV. HgTe QWs are topological insulators with helical edge states when $M < 0$. In the case of $\alpha = 0$, the Hamiltonian is block diagonal. The upper block of Hamiltonian (1) is a time-reversal of the lower block. If the RSOI is absent, we need only to concentrate on the upper block of the Hamiltonian.

In the two-dimensional case, the eigenvalues and eigenstates of the Hamiltonian are

$$\epsilon_\pm = \epsilon_k \pm \sqrt{M^2(k) + A^2k^2}, \quad (2)$$

$$\chi_\pm = N_\pm(Ak\,\mathrm{e}^{\mathrm{i}\theta}, \pm\sqrt{M^2(k) + A^2k^2} - M(k))^{\mathrm{T}}, \quad (3)$$

respectively, where $N_\pm$ are normalization constants, and θ is defined as $\tan\theta = k_y/k_x$ (see Fig. 1(c)) and $k = \sqrt{k_x^2 + \pi_y^2}$. In the presence of RSOI, i.e., $\alpha \neq 0$, the spin-up and spin-down carriers are coupled together, we omit the lengthy expressions for the eigenvalues and eigenvectors here. When the Fermi energy and incident angle θ are fixed, the tunneling process in the presence of vector potential A_y can be viewed as a one-dimensional tunneling process with a one-dimensional effective potential $V_{\mathrm{eff}}(x)$ dependent on A_y.[18] If the Fermi energy is far below the effective potential, the transmission is suppressed. The transmission in the two-dimensional case can be calculated by matching the wave functions and currents at the boundary where $x = 0$ and $x = L$ (see Fig. 1(c)). We assume the wave functions of incident electrons from the left with Fermi wave vector $k_n^{\mathrm{I}} = k_F$ and incident angle θ_n^{I} are $\chi_n^{\mathrm{I}} \mathrm{e}^{\mathrm{i}k_n^{\mathrm{I}}\cos(\theta_n^{\mathrm{I}})x} \mathrm{e}^{\mathrm{i}k_n^{\mathrm{I}}\sin(\theta_n^{\mathrm{I}})y}$. Then, the wave function in the three regions are

$$\begin{aligned} \psi_{\mathrm{I}}(x,y) &= \left[\chi_n^{\mathrm{I}} \mathrm{e}^{\mathrm{i}k_m^{\mathrm{I}}\cos(\theta_n^{\mathrm{I}})x} + \sum_{m=1}^{4} r_m \chi_m^{\mathrm{I}} \mathrm{e}^{-\mathrm{i}k_m^{\mathrm{I}}\cos(\theta_m^{\mathrm{I}})x}\right] \\ &\quad \times \mathrm{e}^{\mathrm{i}k_n^{\mathrm{I}}\sin(\theta_n^{\mathrm{I}})y}, \\ \psi_{\mathrm{II}}(x,y) &= \sum_{m=1}^{4} c_m \chi_m^{\mathrm{II}} \mathrm{e}^{\mathrm{i}k_m^{\mathrm{II}}\cos(\theta_m^{\mathrm{II}})x} \mathrm{e}^{\mathrm{i}k_n^{\mathrm{I}}\sin(\theta_n^{L})y} \\ &\quad + \sum_{m=1}^{4} d_m \chi_m^{\mathrm{II}} \mathrm{e}^{-\mathrm{i}k_m^{\mathrm{II}}\cos(\theta_m^{\mathrm{II}})x} \mathrm{e}^{\mathrm{i}k_n^{\mathrm{I}}\sin(\theta_n^{L})y}, \\ \psi_{\mathrm{III}}(x,y) &= \sum_{m=1}^{4} t_m^{\mathrm{III}} \mathrm{e}^{\mathrm{i}k_m^{\mathrm{III}}\cos(\theta_m^{\mathrm{III}})x} \mathrm{e}^{\mathrm{i}k_n^{\mathrm{I}}\sin(\theta_n^{\mathrm{I}})y}. \end{aligned} \quad (4)$$

By matching the wave functions and currents at $x = 0$ and $x = L$, it follows

$$\begin{cases} \psi_{\rm I}(0,y) = \psi_{\rm II}(0,y), \\ \upsilon_x\psi_{\rm I}(0,y) = \upsilon_x\psi_{\rm II}(0,y), \\ \psi_{\rm II}(L,y) = \psi_{\rm III}(L,y), \\ \upsilon_x\psi_{\rm II}(L,y) = \upsilon_x\psi_{\rm III}(L,y), \end{cases} \tag{5}$$

where υ_x is the x-direction velocity operator given by

$$\upsilon_x = \begin{pmatrix} -2D_+k_x & A & {\rm i}\alpha & 0 \\ A & -2D_-k_x & 0 & 0 \\ -{\rm i}\alpha & 0 & -2D_+k_x & -A \\ 0 & 0 & -A & -2D_-k_x \end{pmatrix}, \tag{6}$$

where $B_+ = B + D$, and $B_- = B - D$. At fixed Fermi energy $E_{\rm F}$ and incident angle θ, the transmission $T(E_{\rm F},\theta)$ can be obtained from Eqs. (4) and (5) using the scattering matrix method.[19] The conductance of the system is $G(E_{\rm F}) = (e^2/\hbar)\int T(E_{\rm F},\theta)\cos\theta {\rm d}\theta$.[17]

3. Numerical results

At the beginning, we investigate the transmission properties in two-dimensional HgTe QWs without RSOI. As shown in Fig. 2, we first plot the transmission $T(E_{\rm F},\theta)$ as a function of $E_{\rm F}$ with $\theta = 0$ and $V_{\rm g} = -10$ meV. When the magnetic field is absent (solid line in Fig. 2(a)), the transmission is almost 2 when the Fermi energy does not lie in energy gaps, i.e., $E_{\rm F} > 10$ meV or $E_{\rm F} < -20$ meV. Note that the perfect transmission is 2 because of the degeneracy of spin-up and spin-down states. The transmission is almost zero between $E_{\rm F} = -20$ meV and $E_{\rm F} = 10$ meV because the Fermi energy is in the gap either in the left and right regions or in the middle region.[15] When the magnetic field is present, the gap in which carriers cannot tunnel grows with the strength of the magnetic fields (see Fig. 2). This suppression is due to the wave-vector filtering effect of the magnetic field.[10,17] We focus on the Fermi energy at which the transmission jumps from nearly zero to almost 2 in the range $E_{\rm F} > 0$ meV. The jump point shifts to higher Fermi energy when the magnetic fields are tuned up (see the dashed, dotted, and dash-dotted lines with $B = 0.3$ T, $B = 0.6$ T, and $B = 0.9$ T, respectively). The jump point shifts with increasing magnetic fields because the effective one-dimensional potential grows with the increasing magnetic fields. If the Fermi energy is below the effective potential, the transmission is almost zero. If the Fermi energy is above the effective potential, the transmission increases significantly. The peaks caused by the constructive interference of propagating modes in the barrier can also be understood in connection with the one-dimensional tunneling process. The peaks have a narrower width in the lower Fermi energy region. The width of the transmission is associated with the lifetime of carriers in the barrier. If the carrier has a lower Fermi energy, then it has lower group velocity and a longer time spent in the barrier, so the transmission peaks at lower Fermi energy have narrower widths. The transmission behavior at $E_{\rm F} < 0$ can be understood in the same way as the carriers treated as holes. The interference between the forward-moving and backward-moving modes in the barrier behaves like Fabry–Pérot (FP) interference in optics. To see the FP interferences more clearly, we plot $T(E_{\rm F},\theta)$ with $E_{\rm F} = 20$ meV and $\theta = 0$ as a function of the barrier length L. When $B = 0$ T and $B = 0.3$ T, the transmission oscillates with L, which is a manifestation of the interferences of FP modes in the barrier. The transmission as a function of barrier length L at $B = 0$ is similar to graphene in the potential barrier, while the transmission at $B = 0.3$ T has the same oscillation behavior as in ordinary 2DEG.[8] When $B = 0.6$ T and $B = 0.9$ T, the transmission is exponentially suppressed because the propagating modes in the barrier are becoming evanescent due to a larger magnetic field. The larger magnetic fields induce an effective one-dimensional potential barrier which is larger than the energy of the incident carriers.

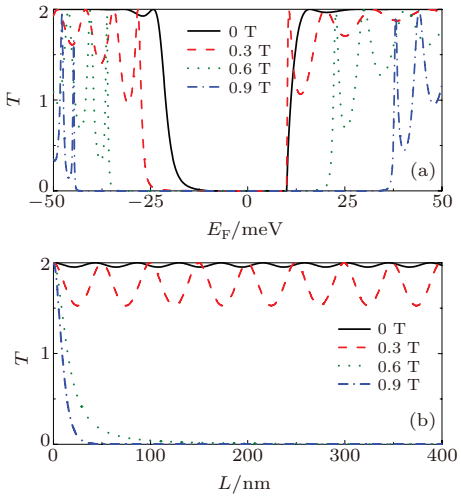


Fig. 2. (color online) (a) Transmission $T(E_{\rm F},\theta)$ as a function of the incident Fermi energy $E_{\rm F}$ at fixed gate voltage $V_{\rm g} = -10$ meV, barrier length $L = 100$ nm, and incident angle $\theta = 0$. (b) Transmission $T(E_{\rm F},\theta)$ as a function of the barrier length L with fixed Fermi energy $E_{\rm F} = 20$ meV, incident angle $\theta = 0$, and gate voltage $V_{\rm g} = -10$ meV.

We next plot $T(E_{\rm F},\theta)$ as a function of θ with fixed $E_{\rm F}$. The transmission is almost perfect at $B = 0$ T (black solid line in Fig. 3(a)) around $\theta = 0$. This is due to the helicity of electrons in HgTe QWs, which prevents backscattering[14] at $\theta = 0$ and is similar to the Klein tunneling in graphene.[8] In graphene, there is no reflection at $\theta = 0$ if there is no intervalley scattering due to the preservation of chirality of Dirac electrons.[8] In HgTe QWs, the perfect tunneling around $\theta = 0$ is due to the helicity of electrons.[15] When the magnetic fields are tuned up, the transmission is suppressed and the resonant tunneling emerges. The transmission is completely suppressed (dash-dotted line in Fig. 3(a)) when the magnetic field is beyond some critical value about $B = 0.81$ T. The transmission behavior as a function of θ can be explained as follows: the effective one-dimensional potential is symmetric with $\theta = 0$ in the absence of magnetic fields and becomes asymmetric when the magnetic fields are included. It can be seen from

Fig. 3(a) that the dashed line has a jump. The angle at which the jump occurs means that the energy of carriers is less than the effective one-dimensional potential at the right side of the jump point and larger than the potential at the left side of the jump point. In Fig. 3(b), we plot the transmission $T(E_F,\theta)$ as a function of gate voltage V_g at $\theta = 0$ and fixed Fermi energy $E_F = 20$ meV. The oscillation emerges when the magnetic field increases and the oscillations show different peak-to-valley ratios between $V_g < 0$ meV and $V_g > 30$ meV. It can be explained as follows. When $V_g < 0$ meV, the states available in the barrier are in the conduction bands and intra-band tunneling occurs; when $V_g > 30$ meV, the available modes in the barrier lie in the valence bands and inter-band tunneling occurs. The valence bands have different dispersions than the conductance bands, so the inter-band tunneling is smaller compared with the intra-band tunneling. The peaks in Fig. 3(b) shift and have different widths at different V_g. The reason for the shift of peaks is related to the shift of levels of quasi-bound states. The gate voltage can shift the position of the levels of quasi-bound states in the barrier, resulting in the shifting of peaks. The width of the tunneling peaks, which become narrower when A_y increases, is due to the wave-vector filtering effect of A_y. We can see that the wave-vector filtering effect shares a similar characteristic with graphene.[10] However, there is a difference in the transmission properties between graphene and HgTe QWs. The graphene has particle–hole symmetry, while in HgTe QWs the particle–hole symmetry is broken. When the barrier is tuned into the hole regime, the transmission is strongly suppressed (see Fig. 3(b)).

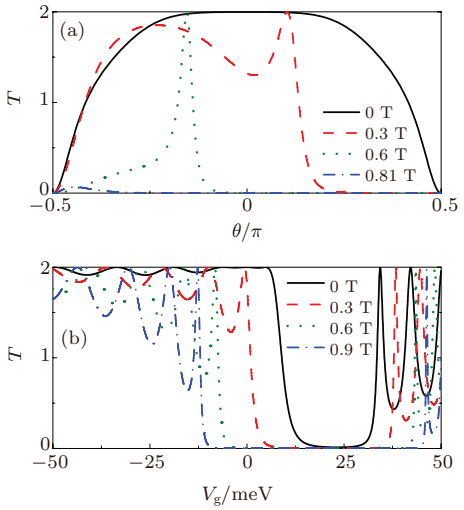


Fig. 3. (color online) (a) Transmission $T(E_F,\theta)$ as a function of the incident angle θ at fixed gate voltage $V_g = -5$ meV, barrier length $L = 100$ nm, and $E_F = 20$ meV. (b) Transmission $T(E_F,\theta)$ as a function of gate voltage V_g with incident angle $\theta = 0$, fixed Fermi energy $E_F = 20$ meV, and barrier length $L = 100$ nm.

Now we turn to study the case where RSOI is present in the middle region. In this case, the degenerate bands of spin-up and spin-down electrons are split into four bands with different dispersions. The RSOI causes different behaviors in the transmission. As shown in Fig. 4(a), the transmission $T(E_F,\theta)$ at $\theta = 0$ still oscillates with E_F, but the peaks are smaller than 2 and are far from perfect tunneling. In Fig. 4(b), we plot the transmission $T(E_F,\theta)$ as a function of barrier length L. There are still FP modes (see Fig. 2(b)), but there is a difference if we focus on the dashed line in Fig. 4(b) and the dotted line in Fig. 2(b). The evanescent behavior for $T(E_F,\theta)$ at $B = 0.6$ T without RSOI is different from the oscillating behavior in the presence of RSOI. In Fig. 4(c), we plot $T(E_F,\theta)$ as a function of θ. The transmission peak in Fig. 3(a) (dotted line) splits into two peaks in Fig. 4(c). In Fig. 4(d), the transmission also shows splits compared to Fig. 3(b). These different behaviors with RSOI in the middle region can be understood as follows. The RSOI induces a splitting in the degenerate bands of spin-up and spin-down carriers with two different Fermi wave vectors k_F^σ ($\sigma = \uparrow,\ \downarrow$). This implies that the two conduction or valence bands have two different k_x^σ ($\sigma = \uparrow,\ \downarrow$) since k_y is the same. Thus, the resonant condition relevant to k_x^σ cannot be satisfied with the same parameters (E_F, L, θ, or V_g) for the two bands. It means that when $k_x^\uparrow$ ($k_x^\downarrow$) meets the resonant condition $k_x L = n\pi$ ($n = 1,2,\ldots$),[8] $k_x^\downarrow$ ($k_x^\uparrow$) cannot satisfy this condition because they are always different. This induces splits in the peaks and departures of peaks from perfect tunneling. The evanescent modes (the dotted line in Fig. 2(b)) in the barrier can become propagating modes (the dashed line in Fig. 4(b)) due to the shift of energy bands. The side peaks are apparent when the peaks are narrow, the lifetime of carriers is long, and the broadened width of quasi-bound energy levels does not cover the side peaks. As shown in Figs. 4(c) and 4(d), the appearance of side peaks is due to the RSOI and wave-vector filtering of magnetic fields. The apparent sub-peaks may suggest an efficient way to detect RSOI in HgTe QWs.

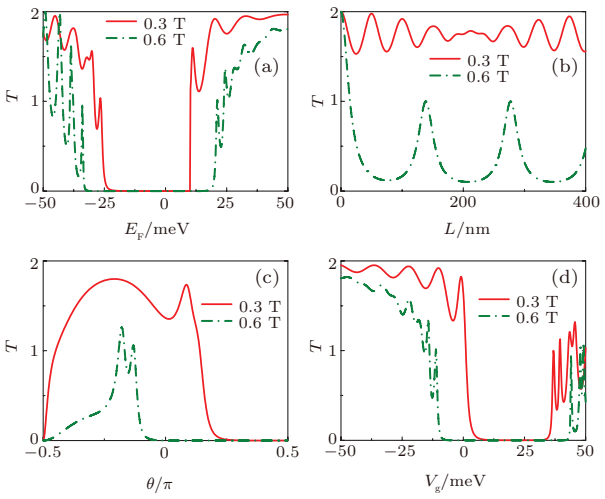


Fig. 4. (color online) Transmission of two-dimensional HgTe QWs with RSOI $\alpha = 50$ meV·nm as a function of (a)E_F, (b) L, (c) θ, and (d) V_g, respectively. The parameters are (a) $L = 100$ nm, $V_g = -10$ meV, $\theta = 0$; (b) $E_F = 20$ meV, $V_g = -10$ meV, $\theta = 0$; (c) $E_F = 20$ meV, $L = 100$ nm, $V_g = -5$ meV; (d) $L = 100$ nm, $V_g = -10$ meV, $E_F = 20$ meV.

4. Conclusion

In summary, we have explored the transmission properties in two-dimensional HgTe QWs with a magnetic–electric barrier. In the absence of magnetic fields, the transmission is perfect around $\theta = 0$ for intra-band tunneling. This is a manifestation of the helicity of electrons in HgTe QWs, which is similar to Klein tunneling in graphene. When the magnetic field is included, the transmission shows a strong wave-vector filtering behavior. The transmission is suppressed and the resonant tunneling behavior emerges. These resonant tunnelings are caused by the quasi-bound states in the electric–magnetic barrier. The positions of these peaks vary with the voltage barrier, the magnetic field, and the barrier length. This wave-vector filtering effect will have potential application in nanodevices based on HgTe QWs. In the presence of RSOI, the peaks in the transmission split and depart from perfect tunneling because of the different wave vectors induced by RSOI.

References

[1] Hasan M Z and Kane C L 2010 *Rev. Mod. Phys.* **82** 3045

[2] Bernevig B A, Hughes T L and Zhang S C 2006 *Science* **314** 1757

[3] König M, Wiedmann S, Brüne C, Roth A, Buhmann H, Molenkamp L W, Qi X L and Zhang S C 2007 *Science* **318** 766

[4] Roth A, Brüne C, Buhmann H, Molenkamp L W, Maciejko J, Qi X L and Zhang S C 2009 *Science* **325** 294

[5] Kane C L and Mele E J 2005 *Phys. Rev. Lett.* **95** 146802

[6] Kane C L and Mele E J 2005 *Phys. Rev. Lett.* **95** 226801

[7] Neto A G, Guinea F, Peres N R, Novosolov K S and Geim A K 2009 *Rev. Mod. Phys.* **81** 109

[8] Katsnelson M I, Novoselov K S and Geim A K 2006 *Nat. Phys.* **2** 620

[9] Novoselov K S, McCann E, Morozov S V, Fal'ko V I, Katsnelson M I, Zeitler U, Jiang D, Schedin F and Geim A K 2006 *Nat. Phys.* **2** 177

[10] Martino A D, Dell'Anna L and Egger R 2007 *Phys. Rev. Lett.* **98** 066802

[11] Silvestrov P G and Efetov K B 2007 *Phys. Rev. Lett.* **98** 016802

[12] Ghosh S and Sharma M 2009 *J. Phys.: Condens. Matter* **21** 292204

[13] Zhai F and Chang K 2008 *Phys. Rev. B* **77** 113409

[14] Zhang L B, Chang K, Xie X C, Buhmann H and Molenkamp L W 2010 *New J. Phys.* **12** 083058

[15] Zhang L B, Zhai F and Chang K 2010 *Phys. Rev. B* **81** 235323

[16] Molenkamp L W, Staring A M, Beenakker C W, Eppenga R, Timmering C E, Williamson J G, Harmans C J and Foxon C T 1990 *Phys. Rev. B* **41** 1274

[17] Masir M R, Vasilopoulos P and Peeters F M 2008 *Appl. Phys. Lett.* **93** 242103

[18] Masir M R, Vasilopoulos P, Matulis A and Peeters F M 2008 *Phys. Rev. B* **77** 235443

[19] Xu H Q 1994 *Phys. Rev. B* **50** 8469

[20] Datta S 1995 *Electronic Transport in Mesoscopic System* (Cambridge: Cambridge University Press)